ULTRASONICS OF NONLINEAR INTERFACES IN SOLIDS: NEW PHYSICAL ASPECTS AND NDE APPLICATIONS

I.Yu. Solodov
Department of Physics, M.V. Lomonosov Moscow State University, Moscow, Russia
solodov@ikp.uni-stuttgart.de

Abstract

The purpose of the lecture is to highlight new physical effects and prospects for NDE-applications of nonlinear acoustics of bounded and imperfect solids that have been developed over the last decade. "Classical" line of investigations is concerned with boundary nonlinearity of ideally bonded interfaces including nonlinear sound reflection, nonlinear propagation of various types of surface and interface waves. The features of acoustic nonlinearity for such an interface are concerned with coupling of elastic modes that results in harmonic generation in a linear solid or, on the contrary, linearisation of an interface between nonlinear solids. A new class of nonlinear phenomena is associated with nonlinear dynamics of non-bonded interfaces and accompanied by gigantic increase in contact nonlinearity due to nonlinear friction and clapping mechanisms. "Non-classical" nonlinear phenomena include subharmonic generation, instability, hysteresis, self-modulation, dynamic chaos caused by nonlinear and parametric resonances of the contact oscillations. A number of case studies considered demonstrate a high potential of acoustic wave interaction with nonlinear interfaces for damage detection, location, and characterisation.

Introduction

A gradual pace of a 30-year history of nonlinear acoustics of solids has been disturbed by a dramatic turn over the last decade. In early 60s, a classical field of investigations was aimed at homogeneous (flawless) crystals whose nonlinearity was associated with lattice anharmonicity. As a result, a unique means was created for experimental characterisation of nonlinear behaviour of inter-atomic forces in crystalline materials [1]. However, even in the first experimental studies a substantial increase in nonlinearity was measured as soon as dislocation pattern was induced in a single crystal of Al by a mechanical impact [2]. Further investigations confirmed an important role of internal boundaries in acoustic nonlinearity enhancement for dislocations in fatigued materials [3] and matrix-precipitate interfaces in alloys [4].

A number of studies were implemented then to find out mechanisms of the boundary nonlinearity using surface acoustic waves (SAW) and interface waves [5-8]. These results were supplemented by direct observations of efficient higher harmonic (HH) generation in bulk acoustic wave reflection from a (bonded) interface between two nonlinear solids [9]. In both cases, the experiments revealed a drastic increase in boundary nonlinearity if a non-bonded contact (two plane surfaces pressed together) was arranged on the path of SAW propagation [5] and in the area of the bulk wave reflection [10]. Besides the much higher efficiency, such a contact acoustic nonlinearity (CAN) was shown to be accompanied by substantial qualitative deviations from classical (lattice) nonlinearity (threshold behaviour, unconventional waveform distortion, fractional subharmonic generation, "self-modulation", instability, chaotic dynamics, etc.) [11-13]. Since such an interface simulates closely an elastic behaviour of a crack, nonlinear acoustics of non-bonded interface became a topical subject of numerous studies and applications concerned with non-destructive evaluation (NDE) of cracked defects.

Another area where the deviations from the classics of nonlinear acoustics were found to be evident was acoustics of rocks [14]. A grainy structure of rocks, apparently, comprises a number of non-ideally bonded interfaces whose nonlinear response dominates in an overall nonlinearity of geomaterials. Different types of contact bonds in the interfaces between grains result in various mechanisms of structural nonlinearity [15] that are involved in interpreting of non-classical manifestations of acoustic nonlinearity in rocks. These mechanisms are complemented by the Preisach-Mayergoyz (P-M) formalism to include hysteresis of elastic properties of rocks [16]. The P-M scheme enables a phenomenological description of such non-classical manifestations like elastic hysteresis and discrete memory observed in static and dynamic experiments as well unconventional features (quadratic (linear) dynamic characteristics for the HHs (resonance frequency shift)) of acoustic wave nonlinear propagation in rocks.

Interestingly, that both of the above approaches though originated from quite different areas (nonlinear acoustics of interfaces and acoustics of rocks) have ultimately come to the similar non-classical developments and a common conclusion that these new nonlinear interface phenomena may become a novel versatile tool (much more practically oriented than its classical predecessor) for acoustic NDE of materials.

The latter fact will be emphasized in this paper: the new physical effects will be considered through the

prism of NDE applications. To place this in historical context, Section 1 will be concerned with ideally bonded nonlinear media where some new properties of the acoustic nonlinearity within surface and interface areas will be shown for nonlinear sound reflection and propagation of boundary acoustic waves. Phenomenology and experimental results on non-classical nonlinear phenomena for non-bonded interfaces are presented in Sections 2 and 3. The case studies of acoustic NDE applications based on the non-classical nonlinear interface phenomena are collected in Section 4.

1. Acoustic nonlinearity of an ideally bonded interface

Nonlinear sound reflection

Consider reflection of vertically polarized shear (S-) acoustic wave of frequency ω from an interface between linear (I) and nonlinear (II) isotropic solids. In the first approximation, the incident wave (from medium I) is accompanied by the mode conversion which results in reflected and transmitted longitudinal (L-) and S-waves.

In the second approximation, the 2ω-waves are produced due to nonlinearity of medium II. The second harmonic field (Fig. 1) comprises four freely propagating L- and S- 2ω-waves in both media whose amplitudes u_α^γ are determined from the second-order boundary conditions of continuity of displacement and generalized stress that can be written in the following general form [7]:

$$\sum_{\alpha,\gamma} a_{\alpha\beta}^{\gamma} u_\alpha^\gamma = N_\beta , \qquad (1)$$

where $\alpha = L, S$; $\gamma = I, II$; $\beta = 1-4$;

Due to the phase matching the matrix $a_{\alpha\beta}^{I,II}$ in (1) is identical to that of the linear solution. The nonlinear 2ω-terms in the right-hand side (N_β) combine the

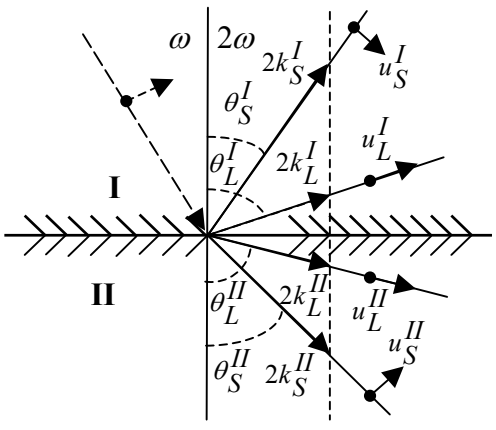

Figure 1: The second harmonic field in SV-wave reflection from nonlinear medium (II).

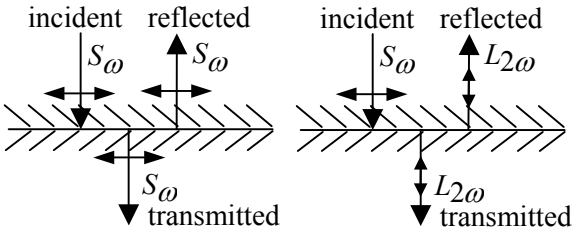

Figure 2: Mode conversion in linear (left) and nonlinear (right) sound reflection.

near-interface located sources produced by the self- and cross-interactions of the linear transmitted L- and S-waves in medium II.

According to (1), elastic coupling makes all modes at the interface nonlinear; the nonlinearity of each mode (u_α^γ) is determined by the cumulative contribution (N_β) of all linear modes that can increase greatly the interface nonlinearity. Due to the elastic coupling, even acoustic waves in the adjacent linear medium acquire nonlinearity. A general solution to (1) in the linear medium can be written as follows [17]:

$$u_\alpha^\gamma = \beta_\alpha^\gamma k_S^I u_0^2 , \qquad (2)$$

where k_S^I is the wave number, u_0 is the amplitude of the fundamental wave and β_α^γ are the nonlinearity parameters of the interface. It shows that for reflected waves no accumulation of nonlinearity takes place and the interface acts as a localized nonlinear source.

Calculations from (2) also demonstrate a high rise in β_α^γ (from ≈ 10 up to $\approx 10^3$) for the reflected second harmonics at the angles of incidence beyond critical values. This increases abruptly the efficiency of the HH generation: as much as 10% of 30 MHz incident wave of moderate intensity ~10 W/cm^2 can be reflected as its second harmonic.

Another interesting feature is concerned with nonlinear mode conversion at the interface. For normal incidence of S-wave (Fig. 2 (right)), the second harmonic field comprises reflected and transmitted L-waves only, while no mode conversion takes place in the linear S-wave reflection (Fig. 2 (left)). If the media across the interface are acoustically matched the reflected second harmonic in Fig. 2 exists even in the lack of linear reflection. This demonstrates a unique opportunity for detection of nonlinear interfaces (cracks) "invisible" with conventional (linear) acoustic instruments.

Nonlinear interface waves

Wave propagation along the interface can be represented as a superposition of reflected and transmitted waves (at complex angles) existing

without the incident wave. In the second approximation, such an approach enables to outline new features of nonlinear waves caused by the specificity of interface nonlinearity [18].

Consider a plane interface between two nonlinear solids assuming their linear elastic properties are close enough to support the interface wave (Stoneley wave (SW)) propagation. System (1) can be adopted to this case by including all cross- and self-interactions of L- and S-waves in both media into the right-hand side terms N_β. In isotropic media, the L-L interactions (only) are resonant and provide a spatial growth of all (partial) solutions u_α^γ in (1). The sum of these partial waves from (1) constitutes the SW second harmonic:

$$\vec{U}_{2\omega}^{\gamma} = U_{L2\omega}^{\gamma}\vec{S}^{\gamma}(2\omega)\exp[i(2\omega t - kx)] \ , \qquad (3)$$

where $\vec{S}^{\gamma}(2\omega)$ are the complex vectors that describe SW displacement field normalized to the amplitudes of L-partial 2ω-wave in the γ-th medium $U_{L2\omega}^{\gamma}$:

$$U_{L2\omega}^{\gamma} = (\omega^2 x/4)\beta_S^{\gamma}U_{L\omega}^{\gamma 2} \ . \qquad (4)$$

The coupled mechanism of the interface wave nonlinearity is manifested in generation of growing HHs of all partial waves due to elastic coupling through the interface that provides nonlinear distortion of the waveform shown in Fig. 3.

The SW nonlinearity parameters in (4) have the form [7]:

$$\beta_S^I = \beta^I + \beta^{II} l_S \ ; \quad \beta_S^{II} = \beta^{II} + \beta^I / l_S \ ; \quad (5)$$

where $l_S = U_{L\omega}^{II}/U_{L\omega}^{I}$ is the elastic coupling factor.

Thus, the nonlinearity of each medium in contact comprises the proper material nonlinearity ($\beta^{I,II}$) and the one induced by the adjacent medium.

Therefore, the boundary nonlinearity of a particular material can be increased substantially by joining it to another material provided all β^γ and l_S are of the same sign. From (5), even a linear material can be made nonlinear by the interface coupling. On the contrary, an interface between nonlinear materials turns linear if $\beta^I/\beta^{II} = -l_S$.

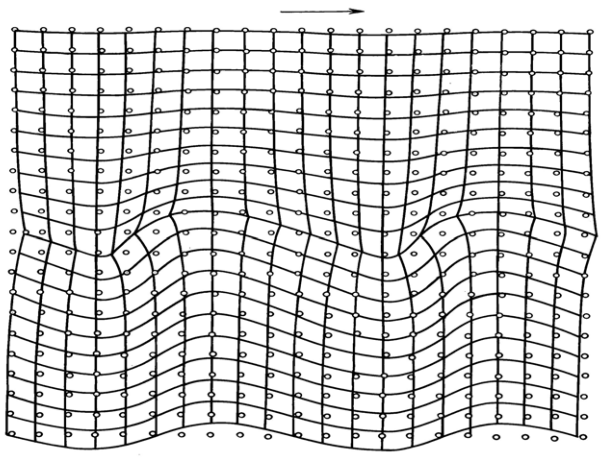

Figure 3: Distortion of acoustic wave form at nonlinear interface.

The coupling nature is a general feature of the interface nonlinearity that manifests in nonlinear propagation of various types of boundary waves (Stoneley-Scholte, Gulyaev-Bleustein, SAW) [19].

2. Acoustic nonlinear phenomena at a non-bonded interface (phenomenology)

Consider a plane interface between two solids whose flat surfaces are in close proximity (open contact) or even touching each other (closed contact). We ignore the surface roughness as well as adhesive bonding forces between surfaces and assume that such a non-bonded interface can be supported by an external static compressive force.

"Clapping" mechanism of CAN (normal traction)

An alternating load applied normally to the interface will find a non-bonded contact stiffness to be asymmetrical: the stiffness for compression is higher than that for tensile stress. Such a "bi-modular" contact can be approximated by the piece-wise stress-strain relation [20] (Fig. 4)):

$$\sigma = C^{II}[1 - H(\varepsilon)(\Delta C/C^{II})]\varepsilon \ , \qquad (6)$$

where $H(\varepsilon)$ is the Heaviside unit step function; $\Delta C/C^{II} = [1 - (d\sigma/d\varepsilon)_{\varepsilon>0}/C^{II}]$ is the stiffness modulation depth that, generally, can be as high as ~1 (against ~10^{-4} in classics).

For $\varepsilon = \varepsilon(t) - \varepsilon^0$, where $\varepsilon(t) = \varepsilon_0 \cos\nu_0 t$ is the input signal and ε^0 is the static contact strain, the stiffness variation from (6) $H(\varepsilon_0 \cos\nu_0 t - \varepsilon^0)(\Delta C/C^{II}) = \Delta C(t)$ is a pulse modulation type function of period $T = 2\pi/\nu_0$ (Fig.

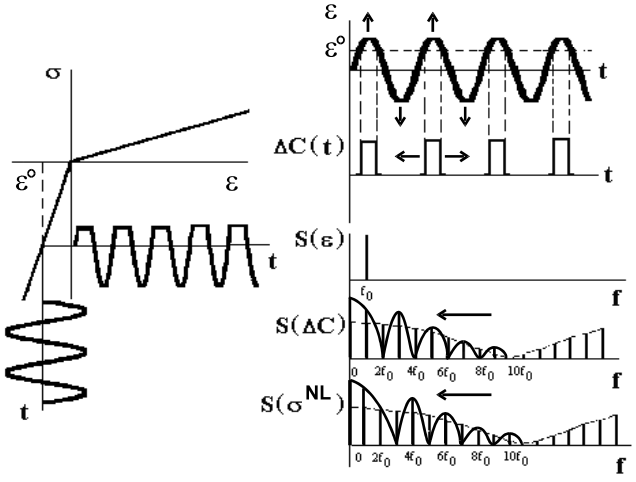

Figure 4: Stress-strain relation and CAN spectrum formation.

4). The spectrum of the nonlinear part in (6): $\sigma^{NL}(t) \sim \Delta C(t)[\varepsilon(t) - \varepsilon^0]$ can be easily found using the modulation theorem and the amplitude of the *n*-th harmonic (*n* = 0, 1, 2, 3...) then takes the form:

$$A_n = \Delta C \Delta\tau \varepsilon_0 \, [sinc((n+1)\Delta\tau) - 2cos(\pi\Delta\tau)sinc(n\Delta\tau) + sinc((n-1)\Delta\tau)] , \quad (7)$$

where $\Delta\tau = \tau / T$ ($\tau = (T/\pi) Arc\cos(\varepsilon^0 / \varepsilon_0)$) is the normalized modulation pulse length.

The spectrum of nonlinear oscillations (7) is also shown in Fig. 4 and contains a number of the HHs (both odd and even) arising simultaneously as soon as $\varepsilon > \varepsilon^0$ (CAN threshold). The harmonic amplitudes are always modulated by the *sinc* envelope function. Its argument depends on τ : as the wave amplitude ε_0 increases, τ grows from 0 to $T/2$ accompanied by corresponding "compression" of the envelope function (Fig. 4). As a result, the CAN HH-amplitudes as functions of ε_0, first, increase monotonically beyond the threshold; then the spectrum "compression" effect causes the amplitude oscillations, unless finally ($\varepsilon_0 >> \varepsilon^0$) it suppresses all odd harmonics (since $\tau = T/2$) [20].

In conclusion we note, that the diode-type CAN also results in nonlinear rectification of the input signal (Fig. 4) that causes the DC-effects (static stress and strain) to appear at the non-bonded interface [21].

Mechanism of nonlinear friction (tangential traction)

Assume now that the surfaces in contact are rough and, therefore, friction coupled for a tangential harmonic load applied. The stress-strain relation becomes nonlinear and hysteretic (Fig. 5): the slanted parts correspond to a joint linear vibration of the interface for $\varepsilon < \varepsilon_1$ (static friction). $\varepsilon < \varepsilon_1$ (static friction). Above this threshold, the kinetic friction force is too small to retain the linearity that initiates sliding and the onset of nonlinearity. The contact stiffness $C(t)$ also changes in a "pulse mode" (Fig. 5)

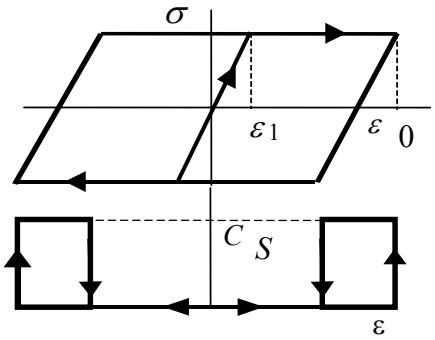

Figure 5: Stress-strain and stiffness variation for tangential traction

twice over the input strain period between C_S (for a „stick" phase) and zero („slide" phase) [22]:

$$C(t) = (C_S / 2)[1 - sign(\dot{\varepsilon})sign[\varepsilon + sign(\dot{\varepsilon})\varepsilon_1]] \quad (8)$$

Similar to the above, $\sigma^{NL}(t) \sim C(t)\varepsilon(t)$ and the nonlinear spectrum is also *sinc*-modulated. However, since $C(t)$ is a $2\nu_0$-function its spectrum consists of even harmonics $2n\nu_0$, while the output spectrum contains odd harmonics $(2n+1)\nu_0$ only.

Impact of bonding forces (normal traction)

The analysis of "clapping" mechanism has been concerned with virtually non-bonded interface and does not include the hysteresis phenomena observed for realistic interfaces (cracks, grains in rocks, etc). To include the hysteresis into dynamics of the interface for normal traction the impact of bonding forces between the surfaces in contact can be considered.

In fact, such a hysteresis is inherent in contact mechanical phenomena in solids and modifies the well-known Hertzian interaction [23]. The attractive adhesive force "sticks" two surfaces prior to any compressive load is applied to the contact while an extra tensile stress is needed to detach the surfaces upon unloading. For rough non-conforming surfaces, such an effect results in the hysteretic interfacial stiffness modulation [24]. Since the stiffness changes twice over the loading period the output nonlinear vibration spectrum, similar to the above, comprises odd HHs only. The adhesive force model [24] is applicable to the interface between soft materials (or soft bonding layers) and can be considered as a good candidate for providing a micro-mechanical mechanism of the P-M units in rocks.

Another approach to taking into account the hysteresis is based on the model of bistable interface (Fig. 6) [25]. The equilibrium position of the open interface (width y_0) is supported by macro-scale elasticity forces between the asperities and stress distribution around the interface. The equilibrium distance for the closed interface (y_c) is due to inter-atomic interaction. As soon as the clapping starts

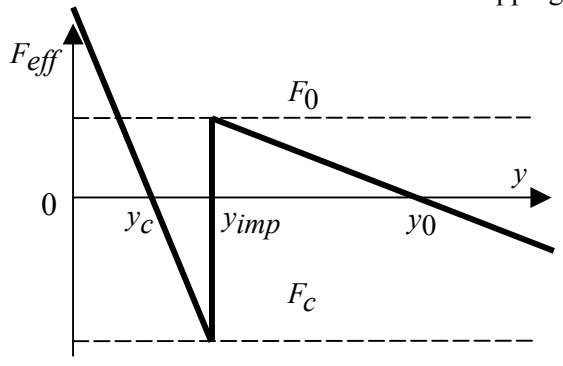

Figure 6: Qualitative model of bonding force for a bistable interface [25].

from the original open position y_0, the average contact width reduces by a jump due to "attraction" by a strong equilibrium position y_c ($F_c >> F_0$). The latter is the reason for the hysteresis: a return to open position takes place at a smaller excitation amplitude.

A striking similarity between the hysteretic bistability effects for the non-bonded interface and those observed for a point contact in atomic force microscopy [26] shows that the nonlinear acoustics of the non-bonded interface can also be a tool for the study of inter-molecular forces in the contact area.

Nonlinear and parametric resonance CAN phenomena

The higher harmonic generation is not the only possible scenario of nonlinear dynamics of cracked defects. The CAN driven defect itself (or a sample with the CAN-defect) can be considered as a nonlinear oscillator. The contact stiffness variation results in a temporal modulation of the oscillator resonance frequencies (parametric modulation) described by the well-known Hill´s and Mathieu´s equations:

$$\ddot{x} + \omega^2(1 + m\cos\nu_m t)x = 0. \qquad (9)$$

Solutions to (9) manifest instability phenomena observed for integer values of $K = 2\omega/\nu_m$, where ν_m is the modulation frequency. The output frequency of the parametric oscillator is [27]: $\omega_{out} = (K + 2n)\nu_m/2$ and vary from the sum of subharmonics (K is odd) to multiple higher harmonics (K is even). The main (strongest) parametric resonance corresponds to K=1 (remember a swing) and results in a series of subharmonics of order 1/2. Dynamic characteristics of parametric oscillations feature a must threshold of the input to compensate the system energy losses followed by an amplitude "jump" (instability) right beyond the threshold.

As the modulation amplitude increases, the resonance values of K deviate from the integer multiples and the parametric resonance can be observed in wide frequency bands. Another factor, which expands greatly the frequency band where the above effects can be observed is concerned with a multiple resonance structure of oscillations. Therefore, e.g. K=1 may correspond to $\nu_m = 2\omega_n$, where $\omega_n = n\omega$ is the n-th resonance frequency . At low values of ω, K=1 may be held for almost continuous variation of the input frequency.

The friction driven CAN displays symmetric stiffness vs. strain distribution (Fig. 5) thus providing $\nu_m = 2\nu_0$. As a result, both odd and even parametric resonances produce only higher harmonics. For "clapping" CAN, the stiffness versus strain is an asymmetric (step-like) function and $\nu_m = \nu_0$. Thus, one may expect multiple subharmonic generation as a result of acoustic wave interaction with "clapping" defects (cracks, delaminations, debonds, etc.).

The subharmonic generation can be modified if one assumes a multi-mode structure of sample (or defect) oscillations (e.g. two eigen-frequencies ω_1 and ω_2). In this case [28], the main parametric resonance can result in simultaneous parametric excitation of a pair of resonance modes $\Omega_1 = n\omega_1$ and $\Omega_2 = m\omega_2$ if the subharmonic of the modulation frequency lies in the middle between them: $\Omega_1 = (\nu_m/2) - \Delta;\quad \Omega_2 = (\nu_m/2) + \Delta$.. Successive nonlinear interaction between ν_m, Ω_1, and Ω_2-components results in a line spectrum with side-lobes around the subharmonics $(2n+1)(\nu_m/2) \pm \Delta$ and near the higher harmonics $n\nu_m \pm 2\Delta$. The presence of the side-lobes is an indication of amplitude modulation (parametric "self-modulation").

Parametric instabilities and the subharmonics of ½-order described by Eq. (9) are particular cases of a more general phenomenon of the nonlinear resonance [29]. The latter comprises a "bend" of the frequency response curve that causes the amplitude "jumps" (threshold instability) as the driving signal frequency (or amplitude) varies. Such "switching" in a two-level oscillating system is accompanied by both frequency and amplitude hysteresis (bistability). If the driving frequency for a nonlinear oscillator (of eigen frequency ω) is ν, then the nonlinear resonance can also take place if $m\nu \pm n\omega = \omega$ and the relation between the input (ν) and the output (ω) frequencies of the oscillator becomes: $\omega = (p/q)\nu$ ($p, q = 1, 2, ..$). Both super- ($q = 1; p > 1$) and subharmonic ($p = 1; q > 1$) resonances are possible that may result in dramatic increase of the HHs and subharmonics (of the *p/q*-order).

Instabilities for the fractional subharmonics and "self-modulation" (spectral side-lobes) develop successively as the driving amplitude increases. Such a spectrum expansion eventually will bring the system into chaotic instability with a noise-like vibration pattern.

3. Non-classical acoustic nonlinear phenomena at a non-bonded interface (experiments)

To demonstrate pertinence of the above phenomenology to the non-bonded CAN phenomena the two sets of experiments will be described. The simulation experiments used an interface between two metal or glass samples with polished (for normal traction) or rough (for friction coupling) surfaces pressed together. An accelerometer or Polytech laser

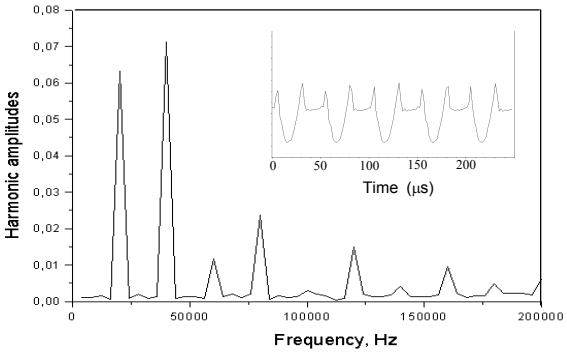

Figure 7: Spectrum and vibration form (insert) for "clapping" interface (20kHz- drive).

vibrometer were used to detect temporal forms and spectra of the interface acoustic vibrations. The results in Fig. 7 clearly demonstrate the "rectified" output and even higher harmonic prevalence predicted above for the "clapping" CAN spectrum.

As expected, the friction coupled interface, on the contrary, shows the odd HH-domination (Fig. 8).

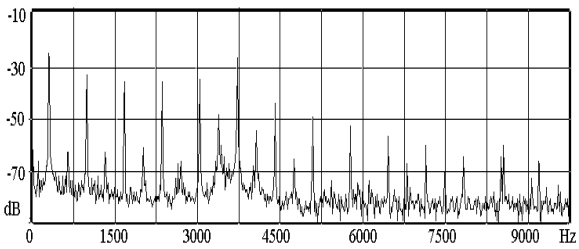

Figure 8: Spectrum of vibrations for friction coupled interface (350Hz-drive).

A linear frequency response of the simulated non-bonded contact for the normal traction drive displayed several peaks in the range of 750-1000 *Hz* with the main resonance at $\cong 800$ *Hz*. As the driving amplitude increases, the nonlinear resonance reveals a step-like rise of the output and in the HH-generation (Fig. 9). The threshold amplitude "jumps", frequency hysteresis and bistability (Fig. 9) correspond to nonlinear resonance "softening" of the contact.

To find out whether propagating acoustic waves can accommodate a diversity of resonance nonlinear oscillation effects described above we studied SAW (frequency range 15 – 45 MHz) interaction with realistic cracks in *YZ-LiNbO₃* . As the amplitude of an acoustic wave incident on the crack increased, a number of super- (2ω and 3ω) and subharmonic ($\omega/2, 3\omega/2, \omega/3, 2\omega/3$) waves were observed in the reflected acoustic field. Their threshold and bistable behaviour (Fig. 10) clearly indicate involvement of nonlinear resonance phenomenon. Above the threshold ($V_{IN} \approx 1.5V$), the sub- and higher harmonics are found to be amplitude modulated ("self-modulation" effect) (Fig. 11). The modulation frequency changes from hundreds of *kHz*

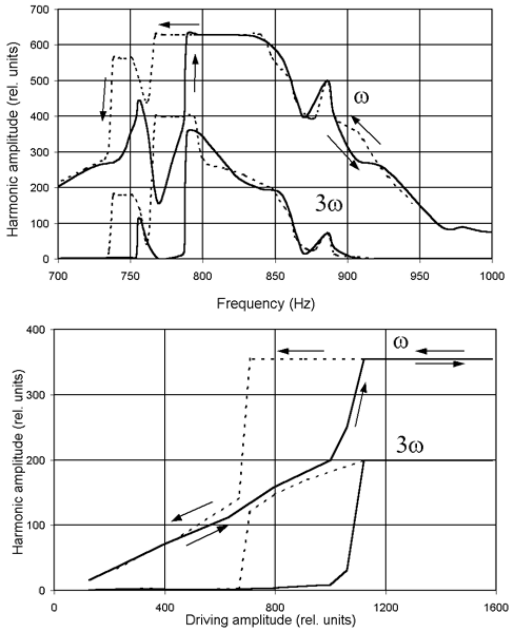

Figure 9: Frequency hysteresis (top) and bistability (bottom) for CAN nonlinear resonance.

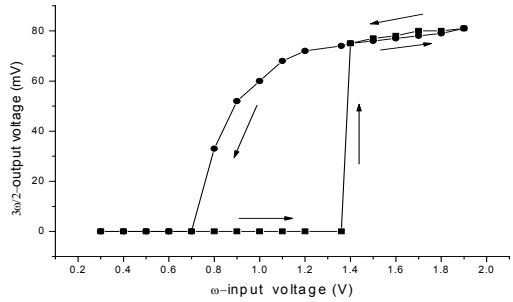

Figure 10: Threshold and bistability for $3\omega/2$ subharmonic in SAW-crack interaction.

to units of *MHz* as the input voltage increases. Beyond the threshold, the amplitude modulation turns into chaotic beats until finally a temporal instability is fully developed and both sub- and super-harmonics change into a noise-like acoustic waves [13].

Note, that similar effects of the threshold and hysteretic behaviour of the HHs and subharmonics have been reported recently also in transmission of bulk acoustic waves in glass sample with cracks [25].

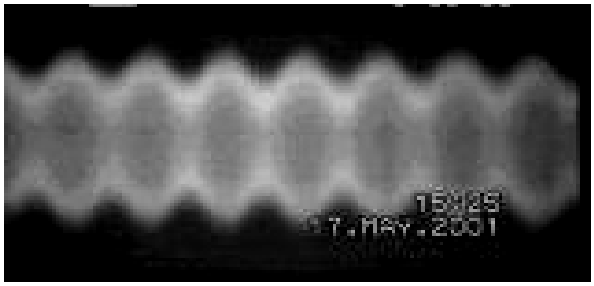

Figure 11: „Self-modulation" effect for $3\omega/2$ subharmonic in SAW-crack interaction.

4. Case studies of non-classical nonlinear NDE of solid interfaces

Experimental features

An overall driving frequency range studied extends from 300 Hz to 45 MHz.. Excitation of low-frequency vibrations (below 20 kHz) was implemented with an electrodynamic shaker (input voltage $\approx 10-15V$); accelerometer (or optical interferometer) used for detection of vibrations followed by FFT or analogue spectrum analysis. To produce 20 kHz intense vibrations, an ultrasound welding piezoelectric stack transducer was driven with a CW electric signal of max power ~ 300W. A scanning laser vibrometer used to detect and image out-of-plane nonlinear excitations. After FFT of the signal detected, the C-scans of sample area are obtained at any spectral line within the frequency bandwidth of 1 MHz. High frequency nonlinear NDE (15-45 MHz-range) employed SAWs generated and detected with interdigital transducers.

Nonlinear reflection mode

It was shown above that the interface areas (including cracks, delaminations, debondings, etc.) are strong nonlinear inhonogeneties for a probing acoustic wave: high local CAN is a source of backward ("reflected") nonlinear excitations even when linear reflection is negligible. This enables detection of small fractured defect "invisible" with linear acoustic NDE and makes the nonlinear reflection defect selective (only nonlinear defects are detected). Fig. 12 illustrates these features of the nonlinear reflection in

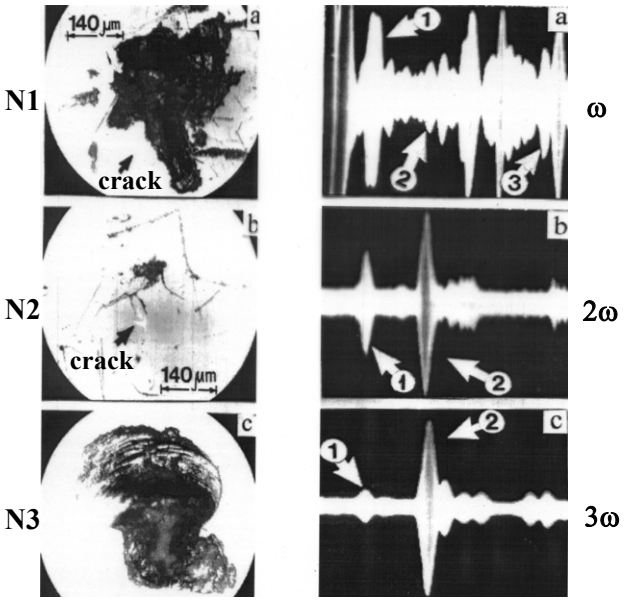

Figures 12 a, b, c: Defect selective acoustic wave nonlinear reflection from surface impact defects. Left: cracked (NN1-2) and hollow (N3) defects; Right: linear (a) and higher harmonic (b, c) reflection.

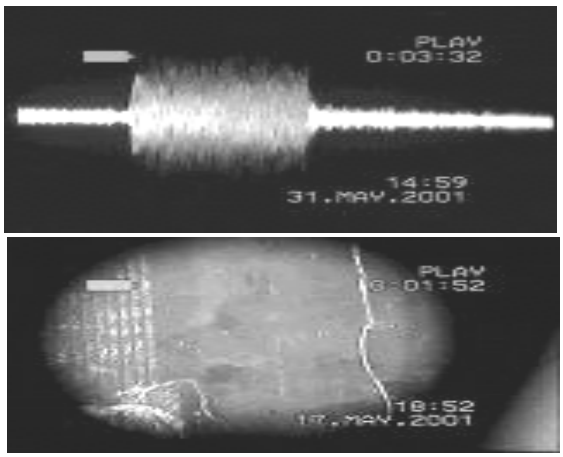

Figure 13. Chaotic mode of nonlinear reflection NDE: noise-like pulse (top) reflected from the surface crack (bottom, right) in $LiNbO_3$ crystal. Electrodes of the SAW transducer (bottom, left) are of 50 μm wide.

detecting cracked surface defects in $LiNbO_3$ crystal [30, 31]. The smallest cracked defect (N2) (almost not visible in linear reflection (a)) dominates in nonlinear reflection (b, c) while a hollow-type (linear) flaw (N3) is ignored.

A strong nonlinear reflection is also observed when a surface crack is irradiated with two surface waves of different frequencies (wave mixing on a crack). For higher input voltages ($\approx 20V$), the subharmonics appear in the reflected field followed by chaotic noise-like nonlinear reflection from a crack (Fig. 13). Figure 13 also shows a small surface crack in $LiNbO_3$ detected in such a "chaotic" mode NDE and invisible with any other reflection modes.

Higher harmonic nonlinear NDE

A high level of HHs generated in a sample due to CAN is an indicator of damage incurred and can be used as a quality assessment test. Moreover, CAN-driven nonlinear excitation originates in a damaged area which, apparently, can be located and imaged in a scanning mode.

Fig. 14 shows the results of acousto-optic HH-imaging of an oval delamination in a "smart structure" (actuator embedded in GFR-matrix). The HH-images selectively reveal the boundary ring of the delamination where "clapping" of the contact surfaces

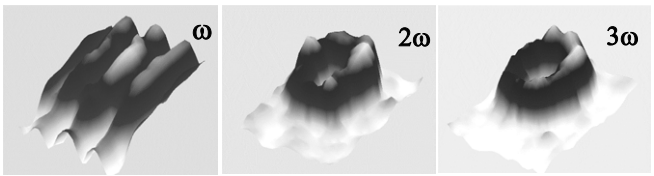

Figure 14: Linear (50 kHz), second and third harmonic images of the delamination area in glass fibre-reinforced (GFR)-composite [32].

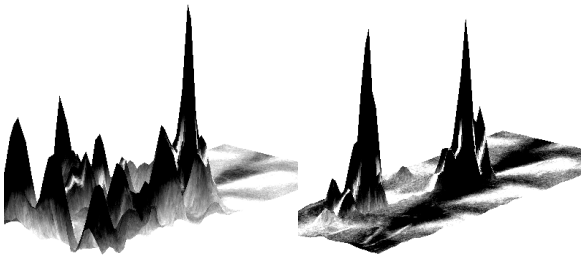

Figure 15: HH-imaging of two clapping areas in a crack: 9th harmonic image (left); 33th harmonic image (right).

is, apparently, expected. Since the HH are generated locally within the "clapping" area one would anticipate the source of nonlinearity to be primarily seen in the nonlinear vibration pattern. On the contrary, the driving frequency (about 50 kHz) image indicates a standing wave pattern over the whole area of the actuator.

The factors that contribute to the local contrast of the nonlinear images include a high input amplitude, acoustic energy trapping inside the defect area and the HH-damping which increases for the higher-order harmonics. In the latter case, one can also avoid the HH-standing wave pattern which distorts the nonlinear images. Fig. 15 illustrates the quality improvement of nonlinear imaging for the higher-order HHs: a precise location of the two clapping areas within the crack is observed only for n>20.

An impact of the input signal amplitude is shown in Figs. 16 a, b for a 4-ply CFRP- sample (15x20 cm) which has an impact in the middle part and a number of edge delaminations. The 10th harmonic distribution clearly shows the positions of all defects; the number of delaminations discerned and the image contrast increase substantially for the higher input.

Nonlinear modulation NDE

By applying a monofrequency excitation it is not unlikely that the driving frequency and its HH match to a linear resonance of the sample and cause standing wave patterns, which smears nonlinear HH-images. To avoid this, a frequency "detuning" in the nonlinear output can be introduced using the wave modulation

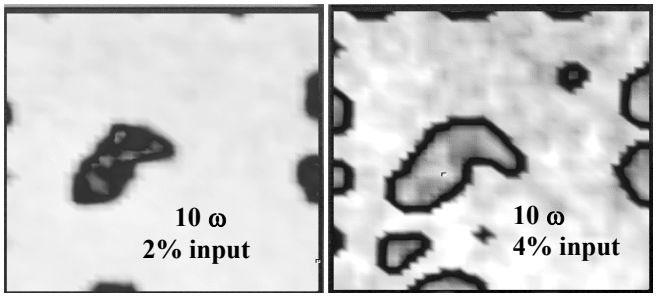

a) b)

Figures 16 a, b: 10th harmonic imaging of the impact (in the middle part) and edge delaminations in CFRP.

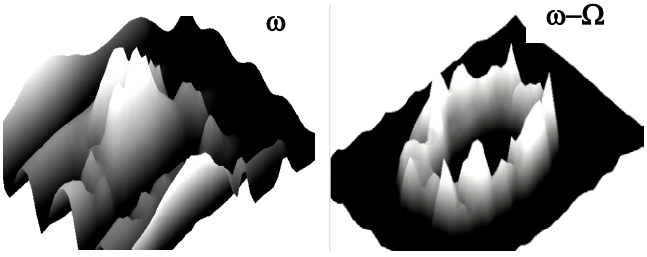

a) b)

Figures 17 a, b: Linear (a) and nonlinear (wave modulation) (b) mages of the delamination area: a) fundamental spectral line 50 kHz; b) difference frequency 49 kHz .

effect. One of its options is to use the amplitude modulation of a high frequency wave (ω) by low frequency (Ω) vibrations. For this purpose, the HH-imaging experiment was complemented by low-frequency vibrations (0.5-5 kHz) of the specimen driven with a shaker. The images in Figs. 17 a, b show that 1 kHz nonlinear detuning from the driving frequency 50 kHz results in a decent image of the delamination.

The nonlinear wave modulation technique was applied for detection of cracking in concrete [33] and fatigue crack imaging in a steel plate [34]. A new mode of the technique that uses cross-modulation between an intense pump wave and a probe signal has been reported recently [35] and applied to crack detection in glass.

Flexibility and application area of the nonlinear acoustic modulation technique expands considerably by combining the benefits of air-coupled ultrasound (remote locating and imaging of defects) with sensitivity of nonlinear methods [36]. Low-frequency vibrations of an interface of a cracked defect (excited with a shaker or a loudspeaker) act like a "shutter" on a transmitted high-frequency focused air-coupled ultrasonic beam. The latter results in a strong amplitude modulation of the transmitted ultrasound by the "clapping" crack interface (nonlinear defect) while a negligible modulation is observed for large and medium scale inclusions and material inhomogeneities (linear defects). Such a defect selective nonlinear NDE is shown in Figs. 18 a-c for a linear (drop of water) and nonlinear (a crack) defects. As one would expect, the linear transmission image clearly reproduces both defects with a comparable contrast

Figures 18 a-c: Air-coupled modulation B-scans of linear (left, a) and nonlinear (right) defects: images at fundamental frequency 452.7 kHz (a); first side-lobe 454.4 kHz- (b) side-lobe 451 kHz (c).

($\Delta V / V \approx -0.6$). On the contrary, the side-band images exhibit a selective rise in the nonlinear output ($\Delta V / V \approx 20$) in the crack area only.

Self-modulation NDE of defects

The parametric "self-modulation" discussed above is a novel opportunity to implement nonlinear NDE and imaging of defects [32]. It is based on parametric excitation of coupled resonances in a damaged sample that results in side-band lines ("satellites") in nonlinear spectrum. Similar to the HH-case, these "satellites" are generated locally within the damaged area and should, therefore, image selectively the source of nonlinearity only. However, unlike all modulation versions mentioned above it uses a single wave (or vibration) which modulates itself parametrically.

Fig. 19 demonstrates the frequency side-lobes in the spectrum of nonlinear vibrations for the sample of multi-ply epoxy-based GFR-composite with an impact. As the input amplitude increases, the spectrum, first, attains HH followed by subharmonics growth, and then supplemented by a number of frequency "satellites" around all spectral lines of vibrations. According to Fig. 19, the self-modulation frequency in this experiment was $\cong 1.2$ kHz.

The defect-selective nature of the self-modulation imaging is illustrated in Figs. 20 a, b, c for the same sample. The linear image taken at the driving frequency 20 kHz reveals a developed standing wave pattern over the whole sample only (Fig. 20 a). The 4th harmonic image of the impacted area (in the centre part of the sample) is also corrupted with the standing wave influence (b). However, a very clear indication of the impact is demonstrated in Fig. 20 c where the image was taken at 198.8 kHz, i.e. at the first side-lobe of the 10th harmonic of the driving frequency. Thus, the "self-modulation" is another way to obtain detuning and diminish the impact of the standing wave pattern in nonlinear acoustic NDE.

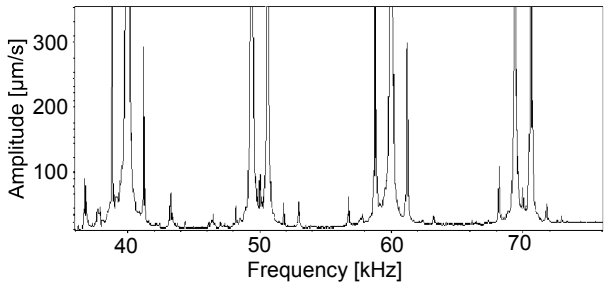

Figure 19: Frequency „satellites" of the HH and subharmonics in vibration velocity spectrum for the GFR-composite with impact: excitation frequency is 20 kHz.

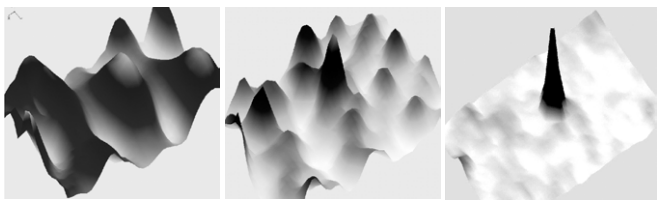

a) b) c)

Figures 20 a, b, c: Self-modulation imaging of the impact area in the GFR-composite: a) linear image (20 kHz); b) 4th harmonic image; c) image at the first side-lobe of the 10th harmonic (198.8 kHz).

The height of the maximum in Fig. 20 c exceeds 20 dB. Vibrometric measurements of the absolute values of vibration velocity enable to estimate the efficiency of the nonlinear frequency transformation: for the fundamental vibration amplitude $\cong 75$ mm/s (the crests in Figure 20 a), the peak value for the 10th harmonic amplitude was $\cong 750$ µm/s and $\cong 600$ µm/s for the 198.8 kHz-side-lobe in the impact area. It shows that the "satellite" generation efficiency is comparable to that of the HH.

Subharmonic NDE

Similar to the self-modulation, the subharmonic generation is caused by a local nonlinear resonance in the defect area and, therefore, can also be used for the defect-selective NDE and imaging. The efficiency of the subharmonic generation strongly depends on the defect parameters and, normally, is substantially lower than that for the HHs. However, our experiments show that for loose cracked defects and delaminations a sufficient level of the subharmonics can be achieved at reasonable input acoustic power.

Fig. 21 shows the subharmonic images of the oval delamination within the "smart structure" in GFR plastic. Comparison with the HH-images of Fig. 14 reveals a higher sensitivity to loose parts (middle area) of the delamination. Some remarkable subharmonic imaging results are obtained for highly dissipative materials like polymers, wood and plywood: high damping prevents the standing wave and results in an exceptional localization of the subharmonics in the defect area [32].

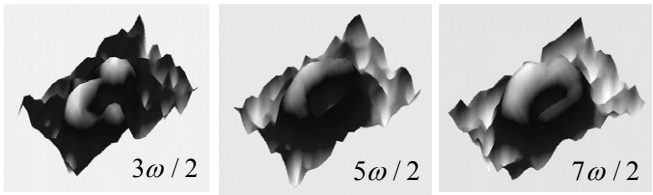

Figure 21: Subharmonic images of the delamination area in GFR-plastic.

5. Conclusions

Acoustic nonlinear phenomena develop in a very specific way at the interface between solids. The nonlinear elastic modes which used to be independent in the bulk of a body become coupled within the interface area. The acoustic nonlinearity of the

interface is determined by overall contribution of the modes allowed to exist at the boundary. Such a nonlinear coupling across the interface can induce nonlinearity in a linear medium or convert the boundary between two nonlinear solids into a linear interface.

The interface bonding is a crucial factor for development of nonlinear acoustic phenomena in inhomogeneous materials. A weakly bonded interface driven by an intense acoustic wave displays a specific nonlinear dynamics and results in an extremely efficient contact nonlinearity associated with either symmetrical or anti-symmetrical stiffness variations.

The sub- and superharmonic resonances strongly affect the interface nonlinear performance and lead to subharmonic generation, instability, hysteresis, self-modulation and dynamic chaos of the nonlinear contact oscillations. Acoustic wave-cracked flaw interplay extends this group of nonlinear oscillation phenomena to propagating wave systems and introduces a new family of non-classical effects in nonlinear (wave) acoustics of solids.

A number of case studies considered demonstrate a high potential of ultrasonic wave interaction with nonlinear interfaces for damage detection, location, and characterisation.

Acknowledgement

The author acknowledges support of the Russian Fund for Fundamental Research (grant N 02-02-1624).

References

[1]. M.A. Breazeale and J. Philip, In*:* Physical Acoustics, v. XVII, Ed. W.P. Mason, Academic Press, New York, 1965.
[2]. A.A. Gedroitz and V.A. Krasilnikov, Sov. Phys. JETP, v. 16, 1122, 1963.
[3]. J.H. Cantrell and W.T. Yost, Phil. Mag., v. A69, 315, 1994.
[4]. J.H. Cantrell and W.T. Yost, J. Appl. Phys., v. 81, 2957, 1997.
[5]. F. Rischbieter, Proc. 5th Intern. Congress on Acoustics, 1965, vol.1, N D13, p. 4.
[6]. R.W. Lardner, J. Appl. Phys., v. 55, 3251, 1974.
[7]. Y. Shui and I. Solodov, J. Appl. Phys., v. 64, 6155, 1988.
[8]. M. Hamilton, D.J. Shull, Yu. A. Il'inskii, E.A. Zabolotskaya, JASA, v. 94, 418, 1993.
[9]. F.M.Severin, I.Yu.Solodov, and Yu.N. Shkulanov, Vestnik Moskovskogo Universiteta, Fisika-Astronomiya., v. 43, N4, 105, 1988.
[10]. Ko Sel Len, F.M. Severin, and I.Yu. Solodov, Sov. Phys. Acoust., v. 37, N6, 610, 1991.
[11]. I.Yu. Solodov, Ultrasonics, v. 36, 383, 1998.
[12]. I.Yu.Solodov and C.A. Wu, Acoust. Phys., v. 39, N5, 476, 1993.
[13]. I.Yu. Solodov and B.A. Korshak, Phys. Rev. Lett., v. 88, 014303, 2002.
[14]. R.A. Guyer and P.A. Johnson, Physics Today, 30, April 1999.
[15]. K.R. McCall and R.A. Guyer, J. Geophys. Res., v. 99, 23887, 1994.
[16]. L.A. Ostrovsky and P.A. Johnson, Nuovo Cimento, v. 24, N7, 2, 2001.
[17]. Y.Zheng, R.Maev, and I.Yu.Solodov, Can. J. Phys., v. 77, 927, 1999.
[18]. I.Yu. Solodov, J. Appl. Phys., v. 64, 2901, 1988.
[19]. Ko Sel Len and I.Yu. Solodov, Sov. Phys.-Acoust., v. 38, N1, 79, 1992.
[20]. I.Yu. Solodov, N. Krohn, and G. Busse, Ultrasonics, v. 40, 621, 2002.
[21]. B.A. Korshak, I.Yu. Solodov, and E.M. Ballad, Ultrasonics, v. 40, 707, 2002.
[22]. E.M. Ballad, B.A. Korshak, I.Yu. Solodov, N. Krohn, and G. Busse, Proc. 16th ISNA, Moscow, 2002, vol. 2, pp. 727-734.
[23]. K.L. Johnson, K. Kendall, and A.D. Roberts, Proc. R. Soc. Lond., A324, 301, 1971.
[24]. C. Pecorary, Ultrasonics, 2004 (in press).
[25]. A. Moussatov, V. Gusev, and B. Castagnede, Phys. Rev. Lett., v. 90, 124301, 2003.
[26]. K. Iganaki, O. Matsuda, and O.B. Wright, Appl. Phys. Lett., v. 80, 2368, 2002.
[27]. Kneubuehl, F. K., Oscillations and waves, Springer, Berlin, 1997.
[28]. A.I. Eller, JASA, v. 53, 758, 1973.
[29]. N. Minorsky, Nonlinear oscillations, D. Van Nostrand Co. Inc., Princeton, 1962.
[30]. I.Yu. Solodov, A.F. Asainov, and Ko Sel Len, Ultrasonics, v. 31, 91, 1993.
[31]. I.Yu. Solodov and A.F. Asainov, In: Nondestructive testing, Eds. V. Hemelrijk & A. Anastassopoulos, Balkema, Amsterdam, 1996, pp. 73-79.
[32]. N. Krohn, K. Pfleiderer, R. Stoessel, I. Solodov, and G. Busse, Proc. Int. Conf. Acoustical Imaging 27, Saarbruecken, 2003 (in press).
[33]. A.A. Stromkov, I.N. Didenkulov, N.M. Kurochkin, and V.V. Chernov, Proc. 16th ISNA, Moscow, 2002, vol. 2, pp. 799-802.
[34]. V.V. Kazakov, A. Sutin, and P.A. Johnson, Appl.Phys.Letts., v. 81, 646, 2002.
[35]. V.Yu. Zaitsev, V.E. Nazarov, V.E. Gusev, and B. Castagnede, Proc. 3d Int. Conf. ETNDT, Thessaloniki, 2003 (in press).
[36]. E.M. Ballad, S.Yu. Vezirov, K. Pfleiderer, I.Yu. Solodov, and G. Busse, Ultrasonics, 2004 (in press).